(19) Europäisches Patentamt
European Patent Office
Office européen des brevets

(11) Publication number : **0 546 961 A1**

(12) **EUROPEAN PATENT APPLICATION**

(21) Application number : **92420412.6**

(51) Int. Cl.[5] : **G02B 6/12**

(22) Date of filing : **12.11.92**

(30) Priority : **14.11.91 US 791830**

(43) Date of publication of application :
16.06.93 Bulletin 93/24

(84) Designated Contracting States :
DE FR GB

(71) Applicant : **EASTMAN KODAK COMPANY**
343 State Street
Rochester, New York 14650-2201 (US)

(72) Inventor : **Strasser, Thomas Andrew, c/o EASTMAN KODAK COMPANY**
Patent Legal Staff, 343 State Street
Rochester, New York 14650-2201 (US)
Inventor : **Hsu, Wei Yung, c/o EASTMAN KODAK COMPANY**
Patent Legal Staff, 343 State Street
Rochester, New York 14650-2201 (US)
Inventor : **Gupta, Mool Chand, c/o EASTMAN KODAK COMPANY**
Patent Legal Staff, 343 State Street
Rochester, New York 14650-2201 (US)

(74) Representative : **Buff, Michel et al**
Kodak-Pathé Département des Brevets et Licences CRT Centre de Recherches et de Technologie Zone Industrielle
F-71102 Chalon sur Saône Cédex (FR)

(54) **A hybrid thin film optical waveguide structure having a grating coupler and a tapered waveguide film.**

(57) A hybrid, thin-film, optical waveguide structure has a substrate (10a) with a grating coupler (12a) formed thereon. A thin-film waveguide film (14a) is formed on the substrate and has a tapered portion overlaying the grating.

FIG.1

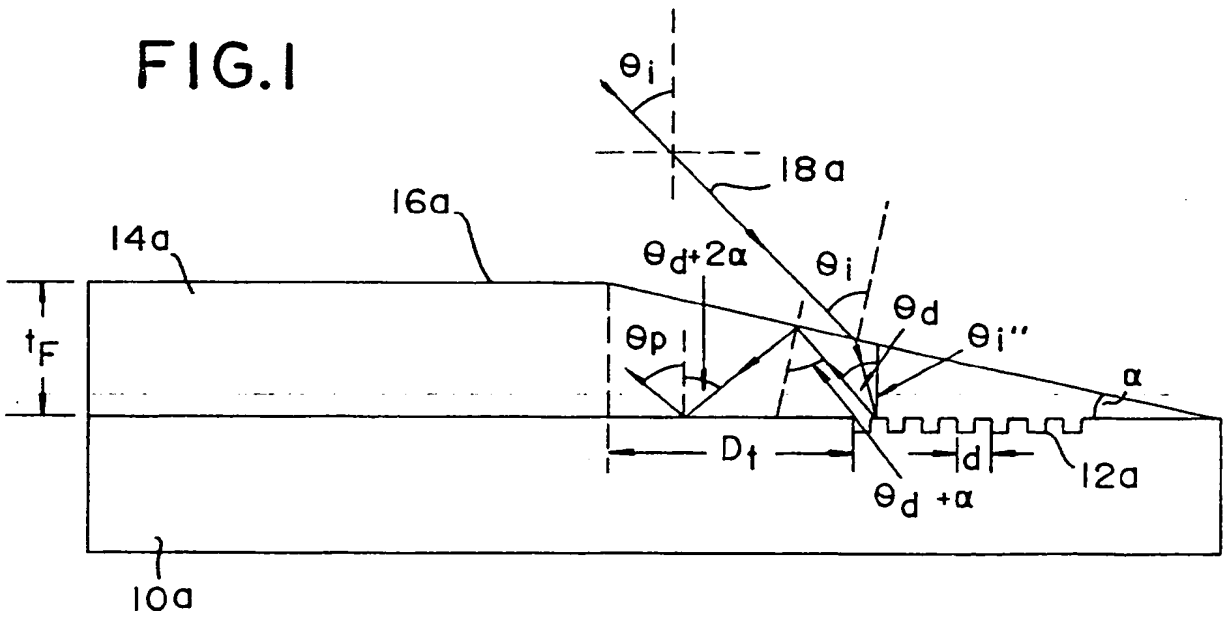

EP 0 546 961 A1

TECHNICAL FIELD

This invention pertains generally to optical waveguide, and, more particularly, to a waveguide structure incorporating a grating coupler.

BACKGROUND OF THE INVENTION

Efficient coupling of a light source into a thin film optical waveguide is a problem for integrated optics devices. The difficulty is maintaining efficient coupling of the light into the waveguide with minimal alignment difficulties. Grating couplers and taper couplers have been utilized for this purpose. Prior grating couplers utilized a grating depth variation to increase the theoretical coupling efficiency.

A grating coupler couples the light by diffracting an incident beam off a grating on the surface of the waveguide either into or out of the planar waveguide, depending on whether it is used as an input or an output coupler. The main disadvantage of the grating coupler is that efficient coupling is obtained only over a narrow range of wavelength and/or incidence angles. In current optical diode laser applications, it is difficult to use grating couplers because of beam divergence and wavelength instability. Accordingly, it will be appreciated that it would be highly desirable to have an optical diode laser structure wherein it is easy to use grating couplers, and wherein the difficulties with beam divergence and wavelength instability are eliminated.

A taper coupler couples the light either into or out of the film by total internal reflection of the beam off of a taper in the film waveguide. The reflection of a propagating beam in the taper changes the propagation angle in the waveguide, either changing an input beam toward the mode propagation angle within the waveguide, or changing a mode propagating in the waveguide. The mode propagating in the waveguide is changed to an angle less than that for total internal reflection at the waveguide/substrate interface, and the beam is then outcoupled into the substrate. A characteristic of this coupler is that the beam outcoupled from the waveguide is spread over a wide angular range of 10° or more, compared to the grating input coupler which is spread over an angular range of 1° or less. The main problem for input coupling is mode matching, which is very difficult to achieve due to a complex relationship between beam divergence and the intensity distribution. A difficulty for output coupling is that the outcoupled beam cannot be collimated or imaged clearly, therefore, it is difficult to utilize the beam for functions other than simple intensity detection. Accordingly, it will be appreciated that it would be highly desirable to have a structure wherein mode matching can be achieved and the outcoupled beam can be collimated or imaged clearly.

SUMMARY OF THE INVENTION

The present invention is directed to overcoming one or more of the problems set forth above. Briefly summarized, according to one aspect of the present invention, a hybrid optical waveguide structure comprises a substrate having a grating formed thereon, and a thin-film waveguide film formed on the substrate and having a nonlinear portion overlaying the grating.

The combination of a grating with a tapered film yields a hybrid coupler that couples light efficiently, with an incidence angle or wavelength acceptance that is altered by the taper structure.

A tapered waveguide film is deposited on a substrate with a grating structure resulting in a hybrid thin film waveguide coupler designed for a broader or narrower acceptance for wavelength or incidence angle. The couplers are as efficient as traditional grating couplers but with much broader acceptance. The maximum broadening is a coupling full-width-half-maximum (FWHM) of 2° (or 12 nm). This is several times the acceptance of an untapered structure.

These and other aspects, objects, features and advantages of the present invention will be more clearly understood and appreciated from a review of the following detailed description of the preferred embodiments and appended claims, and by reference to the accompanying drawings.

BRIEF DESCRIPTION OF THE DRAWINGS

Figure 1 is a diagrammatic sectional view of a preferred embodiment of an optical waveguide structure constructed according to the present invention utilizing a hybrid grating to tapered film coupler for broadening the acceptance of the grating coupler.

Figure 2 is a diagrammatic sectional view of another preferred embodiment of an optical waveguide structure similar to Figure 1, but illustrating a hybrid grating to tapered film coupler for narrowing the acceptance of the grating coupler.

Figure 3 is a diagrammatic sectional view of an optical waveguide structure illustrating a linear profile used

in ray tracing calculations along with the definition of the D_t and z_0 parameters for the linear profile.

Figure 4 is a diagrammatic sectional view of an optical waveguide structure similar to Figure 3, but illustrating a cosine profile used in ray tracing calculations along with the definition of the D_t and z_0 parameters for the cosine profile.

Figure 5 is a diagrammatic sectional view of an optical waveguide structure similar to Figures 3 and 4, but illustrating an exponential profile used in ray tracing calculations along with the definition of the D_t and z_0 parameters for the exponential profile.

Figure 6 graphically illustrates Θ_p vs. Θ_i dependence from ray tracing for a cosine profile with $\lambda = 0.6328$ μm, $d = 0.36$ μm, $n_0 = 1.0$, $n_s = 1.46$, $n_f = 2.3$, and $t_f = 0.20$ μm, and illustrates the D_t dependence for a given taper of length $z_0 = 1000$ μm, with $D_t = 250$, 500, and 750 μm.

Figure 7 graphically illustrates Θ_p vs. Θ_i dependence from ray tracing for a cosine profile similar to Figure 6 with $\lambda = 0.6328$ μm, $d = 0.36$ μm, $n_0 = 1.0$, $n_s = 1.46$, $n_f = 2.3$, and $t_f = 0.20$ μm, but illustrates the z_0 dependence for the constant taper input position $D_t = 300$ μm, and $z_0 = 400$, 600, and 1200 μm.

Figure 8 graphically illustrates the Θ_p vs. Θ_i calculated by ray tracing for the linear, cosine and exponential profiles with a constant taper ratio, D_t/z_0, of 0.5 assuming l = 0.6328 μm, $d = 0.36$ μm, $n_0 = 1.0$, $n_s = 1.46$, $n_f = 2.3$, and $t_f = 0.20$ μm.

Figure 9 graphically illustrates the normalized taper slope $d(t/t_f)/d(z/z_0)$ as a function of taper position for the linear, cosine, and exponential curves of Figure 8 with the input position of $D_t/z_0 = 0$ 5 shown and with propagation toward the waveguide taking place to the left toward $z/z_0 = 0$.

Figure 10 graphically illustrates the experimentally measured relative coupling efficiency η vs. incidence angle Θ_i for a 0.2 μm ZnS film on quartz.

Figure 11 graphically illustrates the calculated dispersion relation Θ_p vs. Θ_i for different taper ratios for a grating-to-tapered film coupler wherein is overlaid the propagation angle axis the η vs. Θ_p dependence from Figure 10.

Figure 12 graphically illustrates the calculated cutoff thickness for the TE_1 mode vs. film refractive index, n_f, for films on quartz (n = 1.46) with $\lambda = 0.6328$ μm.

Figure 13 graphically illustrates the maximum propagation angle of TE_0 single mode waveguide as a function of the films' refractive index for films on quartz (n = 1.46 and $\lambda = 0.6238$ μm) using the effective refractive index results shown in Figure 12.

Figure 14 graphically illustrates the calculated angular dispersion of the coupler $d\Theta_p/d\Theta_i$ at the coupling angle of incidence as a function of the taper ratio with different film refractive indices (n_f = 1.7, 2.0, and 2.3) shown to compare the acceptance-broadening capability of different films.

Figure 15 graphically illustrates the angular dispersion of the coupler $d\Theta_p/d\Theta_i$ shown as a function of taper ratio D_t/z_0 for different grating periods (d = 0.36, and 0.32 μm).

Figure 16 graphically illustrates the film thickness measured by a profilometer of a taper fabricated by vacuum deposition as a function of position on the taper.

Figure 17 illustrates the geometry of the samples fabricated wherein both a tapered and an untapered grating result on the same waveguide.

Figure 18 graphically illustrates the coupling efficiency η as a function of incidence angle Θ_i for the first ZnS sample.

Figure 19 graphically illustrates the coupling efficiency characteristics of the more sharply tapered ZnS sample of Figure 18 for the η vs. Θ_i characteristics of the untapered grating.

Figure 20 graphically illustrates the coupling efficiency characteristics of the more sharply tapered ZnS sample of Figure 18 similar to Figure 19, but for the η vs. Θ_i characteristics of the taper grating at a taper ratio of 0.55.

Figure 21 graphically illustrates the coupling efficiency characteristics for a taper coupler fabricated with a polycarbonate film.

DETAILED DESCRIPTION OF THE PREFERRED EMBODIMENTS

Referring now to the drawings, Figures 1 and 2 illustrate the coupling structures of the present invention. Figure 1 shows a coupling structure having a substrate 10a with a grating 12a. A waveguide film 14a of general thickness t_f is disposed on the substrate 10a, and a cover medium 16a is disposed on the waveguide film 14a. The waveguide film 14a tapers from a general thickness, t_f, to a thickness of about zero in the area of adjacency of the film 14a and grating 12a.

Figure 2 similarly shows a coupling structure having a substrate 10b with a grating 12b. A waveguide film 14b of general thickness t_f is disposed on the substrate 10b, and a cover medium 16b is disposed on the waveguide film 14b. The waveguide film 14b increases from a general thickness, t_f, to a thickness greater than

thickness t_f in the area of adjacency of the film 14b and grating 12b. The thickness increase creates a taper in the region of the grating 12b. At the end of the taper, the film 14b preferably has another region of uniform thickness, t_f.

An incident beam 18 is diffracted off the grating 12 at the interface of the waveguide 14 and substrate 10. The diffracted beam undergoes total internal reflection off the tapered portion of the guiding film 12. The taper changes the propagation angle within the waveguide such that upon leaving the tapered region, the beam is traveling at the correct propagation angle for the guided mode.

The taper changes the angular acceptance of the grating coupler 12 through two effects. The first effect is that a beam diffracted from the grating undergoes different numbers of bounces off the taper, depending on the diffraction angle. Because each bounce changes the propagation angle in the waveguide, bouncing can be used to compensate for the changes in propagation angle with incidence angle.

The second effect is that the shift induced by the bounces changes the coupling angle of incidence When so designed, this can lower the value of the angular dispersion of the grating, reducing change in diffraction angle due to change in incidence angle.

The effect of the taper on the grating coupler in Figure 1 will now be considered in order to optimize the acceptance-broadening due to the taper. The following descriptions can be applied to the acceptance-narrowing configuration of Figure 2 by reversing the sign of the taper angle, α. The taper angle, α, is, as illustrated, the angle of incline or decline of the tapered portion of the waveguide film 14 relative to the grating 12 and substrate 10. The angle α is positive when the film thickness, t_f, is decreasing in the grating area near the end of the taper, and negative when the film thickness, t_f, is increasing in the grating area near the end of the taper.

Referring to Figure 1, the final propagation angle, Θ_p, is calculated in the waveguide as a function of the angle of incidence from air, Θ_i, using a ray tracing program, for example. This enables an evaluation of the theoretical acceptance range because waveguide mode will only support a fixed range of propagation angles. The ray tracing approach assumes an infinitesimally small beam diameter that is diffracted from the edge of the grating at a taper distance, D_t, from the end of the tapered region.

Referring to Figures 1-5, the effect of a linear taper of angle α on the diffracted beam is shown in Figure 1. The beam diffracted at an angle Θ_d relative to the substrate normal is incident at the taper interface at an angle $\Theta_d + \alpha$ due to the taper. Given that the reflected angle is equal to the incidence angle, the reflected beam will be incident at the substrate interface at an angle of $\Theta_d + 2\alpha$ relative to the substrate normal. This 2α increase in propagation angle will occur for every reflection off the taper surface. The net result is a shift of $2\alpha n$, where n is the number of bounces off the taper surface. The taper distance, D_t, is the distance from the edge of the diffraction grating to the end of the taper. The shift due to the taper is dependent on the number of bounces off the taper, and more taper bounces result from longer taper distances. The maximum limit on the taper distance is determined by the taper profile. The taper length, z_0, is the full length of the taper, as shown in Figure 3. This is related from geometry to the previous α angle by

$$z_0 = \frac{t_f}{\tan(\alpha)} \quad (1)$$

where t_f is the waveguide film thickness. Neglecting the finite size of the beam, the maximum taper distance, D_t, is z_0. The effect of the linear taper is therefore described by the taper length, z_0, and the taper distance, D_t. Equation (1) is for linear tapers, but it is useful to determine average value of α for other taper profiles.

Three different taper profiles were considered because the tapers fabricated were not linear. Experimentally, tapers which were formed by a shadow in vacuum deposition were found to have a taper profile similar to a cosine function (Figure 4). Tapers formed by dip coating methods were found to approximate an exponential decay in thickness across the taper (Figure 5). The waveguide film thickness, t_f, as a function of position, z, for each of the profiles depends on the taper length, z_0. The definition of z_0 for these different profiles is made with the idea of this being the maximum taper distance, D_t, that is allowed.

The range of possible angles of incidence are determined by the requirement that the diffracted beam remain in the waveguiding film. The angle of the diffracted beam can be calculated from the general grating diffraction equation.

$$n_i \sin(\Theta_i) + n_d \sin(\Theta_d) = \frac{m\lambda}{d}, \quad (2)$$

where Θ_i is the angle of incidence, Θ_d is the diffracted angle, m is a positive integer, λ is the wavelength of the diffracted beam, d is the period of the diffraction grating, and n_i and n_d are the refractive indices of the incident and diffracted media, respectively. These variables are shown in Figure 1 where Θ_i'' is the incidence angle within the substrate, and the refractive indices, n_i and n_d, each equal n_f because the incidence and diffraction of interest occurs in the film. For the diffracted beam to remain in the waveguiding film, there must be a real solution to equation (2) (e.g., $\Theta_d \leqq 90°$). When $\Theta_d = 90°$ is substituted into Eq. (2), the result is the maximum angle of incidence, Θ_i'', for diffraction to occur. The minimum angle of incidence is determined by the diffraction angle at

which total internal reflection no longer occurs at the interface of the film and substrate (e.g., the grating couples into a substrate mode). The critical angle, Θ_c, for the interface is

$$\Theta_c = \text{asin} \left(\frac{n_s}{n_f}\right). \quad (3)$$

Θ_c can be substituted for Θ_d in Eq. (2) to get the maximum angle of incidence for a diffracted beam to remain confined in the waveguide film.

The relationship between the measurable angle of incidence in air and the limiting angles of incidence at the grating can be determined. By retracing the beam incident on the grating back to the taper surface, it is found that the incidence angle just inside the film, Θ_r, can be expressed as

$$\Theta_r = \Theta_i'' + \alpha. \quad (4)$$

The beam at the taper interface has undergone refraction according to Snell's law

$$\sin(\Theta_i') = \frac{n_f}{n_0} \sin(\Theta_r), \quad (5)$$

where n_0 and n_f are the indices of the media as shown in Figure 1, and Θ_i' is the incidence angle relative to the taper normal. The conversion of the incidence angle relative to the substrate normal, Θ_i, can be expressed as

$$\Theta_i = \Theta',^i - \alpha. \quad (6)$$

The relation of the angle of incidence in the cover medium, Θ_i, to the angle of incidence in the film,

$$\Theta'',^i,$$

is given by the combination of Eqs. (4) - (6). This can be combined with Eqs. (2) and (3) to find the initial diffraction angle, Θ_d, for a given air incidence angle, Θ_i.

The effect of coupling was evaluated using a ray tracing approach. These results are expressed as angular dispersion curves Θ_p vs. Θ_i in Figures 6-8 for different coupler structures wherein Θ_p is the propagation angle. The propagation angle within the taper is increased by 2α for each bounce off the taper; where α is a function of z for nonlinear tapers. The ray tracing program calculates the final propagation angle in the waveguide, Θ_p, after the beam traverses the tapered region. This calculation with equations 2-6 was performed for the range of incidence angles that had a trapped diffracted beam.

For a cosine taper with z_0 = 1000 μm, and D_t = 250, 500 and 750 μm, the results are shown in Figure 6. The untapered result, D_t = 0, is also shown for comparison. The angular shift due to the taper increases the propagation angle thereby decreasing the Θ_i necessary to obtain a given Θ_p. With increased taper distance, D_t, the propagation angle for a given incidence angle increases further.

The dispersion results were calculated for a cosine profile with D_t = 300 μm, and z_0 = 400, 600, and 1200 μm as shown in Figure 7. Increasing the taper length, z_0, decreases the propagation angle for a given incidence angle. In comparing Figures 6 and 7, it is not the magnitude of D_t or z_0 that is of interest, rather the taper ratio D_t/z_0. This can be seen by comparing the D_t = 500 μm line in Figure 6 with the z_0 = 600 μm line in-Figure 7. These two tapers have a D_t/z_0 ratio of 0.5, and, notwithstanding that the tapers are of different lengths, the Θ_p vs. Θ_i dependence is identical. Qualitatively, the taper ratio may be viewed as essentially the percentage of the taper that is utilised in shifting the propagation angle within the taper.

Referring to Figure 8, the effects of different taper profiles on the propagation angle are shown. The untapered Θ_p vs. Θ_i plot is shown as well as that for linear, cosine, and exponential tapers, each with a taper ratio, D_t/z_0 of 0.5. While the taper ratio describes the shift for any given profile, the amount of shift is also dependent on the profile itself. There is dependence because the average value of the taper angle α changes with the profile, depending on what portion of the taper is being used. Therefore, when α, which is a function of z, has a higher average value between the input position on taper and the beginning of the waveguide, a larger taper

shift results.

Referring now to Figure 9, the normalized taper angle as a function of taper position for the different profiles calculated is shown. Although the exponential profile has the smallest value for α at $z/z_0 = 0.5$, the average value of α between z/z_0 of 0.5 and 0 is larger than that for the linear and cosine profiles. Therefore, as expected from Figure 8, the exponential profile shows the largest taper shift. Even though the several profiles have different taper shifting at the same taper ratio, variation of the taper ratio allows equivalent taper shifts and acceptance-broadening to be achieved using any of the taper profiles. The profile shape must be considered for design, but any well-controlled profile shape is adaptable.

To optimize the taper structure, acceptance-broadening resulting from the taper shift needs to be calculated. All angular broadening results can be recast as wavelength broadening results using the grating relationship between Θ_l and λ given in the grating diffraction equation, Eq. (2). To determine the acceptance-broadening due to the taper, the acceptance of a traditional grating coupler must be known. The coupling efficiency η measured as a function of incidence angle Θ_l for a grating coupler is shown in Figure 10. Using Eq. 2, Θ_l is converted to the mode propagation angle Θ_p within the waveguide. The range of propagation angles is broader than the theoretical single propagation angle because the finite size and divergence of the laser beam give rise to a slight broadening. Assuming that propagation angle dependence is the characteristic acceptance of the waveguide structure for the particular beam used (1 mm collimated beam) and that it is independent of the type of coupler used to get the light into the waveguide. Then, because the η vs. Θ_p curve is taken to be a constant for the given waveguide and laser beam, angular broadening in the η vs. Θ_l curve must be accomplished by reducing the angular dispersion of the coupler, $d\Theta_p/d\Theta_l$, at the coupling angle of incidence. Reduction of the angular dispersion of the coupler has been shown in the Θ_p vs. Θ_l ray tracing results for Figures 4 and 5.

Figure 11 illustrates a conversion to acceptance-broadening, which is a Θ_p vs. Θ_l plot for various taper ratios. Superimposed on Figure 11 is a plot of the intrinsic mode width. The broadening in incidence angle is illustrated for different taper ratios by the superposition of the efficiency plot onto the angular dispersion curves. Taper shifting above the optimum taper ratio $D_t/z_0 = 0.57$ yields final propagation angles that cannot match the intrinsic propagation angle. Maximum broadening occurs with the taper that has the minimum angular dispersion at the propagation angle for the mode being coupled. This occurs at the minimum in allowable incidence angle near the substrate mode. The variable which describes the broadening effect of the hybrid coupler is the angular dispersion at the coupling angle, $(d\Theta_p/d\Theta_l)\Theta_p = \Theta_m$, henceforth referred to as the coupler dispersion. Because the angular dispersion curves are approximately linear over the angular range of interest, Figure 11 provides an accurate figure of merit for comparing different coupler structures.

The following experiments used substrates of quartz, with index $n_s = 1.46$, and cover media of air, with index $n_0 = 1.0$. The film refractive index n_f and the grating period d were the variables left to optimize.

To maximize the acceptance width of the coupler, the angular dispersion of the coupler $d\Theta_p/d\Theta_l$ should be minimized. The previous ray tracing results of Figure 11 illustrate that the minimum dispersion for any taper ratio occurs near the coupling angle for the substrate mode which is the minimum angle of incidence. Further, for couplers that couple at the minimum angle of incidence, the dispersion decreases with higher taper ratios. To obtain coupling at the minimum angle of incidence and higher taper ratios D_t/z_0, the intrinsic mode propagation angle Θ_m of the waveguide should be maximized. Because the intrinsic mode propagation angle is proportional to the waveguide thickness t_f, the waveguide thickness should be maximized to minimize dispersion. To maximize the intrinsic mode propagation angle for TE single mode waveguides, the thickness of the waveguide was taken to be the cutoff thickness of the TE_1 mode which is the maximum allowable waveguide thickness while maintaining only one mode.

Referring to Figures 12-14, the cutoff thickness for the TE_1 mode was calculated for film refractive indices between 1.5 and 2.5. The effective index, n_{eff}, was then calculated using the cutoff thickness, the cover, substrate and film indices, and wavelength. The effective index and the film index were used to calculate the mode propagation angle within the waveguide, $\Theta_m = \sin^{-1}(n_{eff}/n_f)$, for the range of film refractive index (Figure 13). Film refractive indices of 1.7, 2.0, and 2.3 were chosen for the angular dispersion calculations. The coupler dispersion, $(d\Theta_p/d\Theta_l)\theta_p = \theta_m$, was then calculated as a function of the taper ratio D_t/z_0 using the ray tracing program. These coupler dispersion functions for the three different film refractive indices are shown in Figure 14. It can be seen from Figure 14 that the higher film refractive index reduces the angular dispersion and therefore broadens the angular acceptance of the coupler. The relative broadening is defined here as the coupler dispersion $(d\Theta_p/d\Theta_l)\theta_p = \theta_m$ for the optimum taper ratio $D_t/z_0 = 0.57$ over that for zero taper $D_t/z_0 = 0$. The highest film refractive index 2.3 shows the most relative broadening, about 4.3X, compared to 4.0X for $n_f = 2.0$ and 3.5X for $n_f = 1.7$. Therefore, the higher the film refractive index, the broader the angular acceptance.

Referring to Figure 15, the coupler dispersion was also calculated for two grating periods that were available for experimentation, d = 0.32 μm and 0.36 μm. The coupler dispersion vs. taper ratio is plotted for these periods in Figure 15. Generally, the dispersion decreases with the grating period. A decrease in the grating period can

affect the coupler diffraction efficiency. Efficiency losses should therefore be considered when decreasing the grating period to broaden acceptance. Although no attempt was made to optimize the efficiency of the grating to taper couplers, the efficiencies measured experimentally were equal for tapered and conventional grating couplers. To optimize the grating to tapered coupler efficiency, there are additional considerations for previous grating coupler designs. One consideration is that the coupling angle of incidence is shifted by the taper. A second consideration is that the effective refractive index at the point of coupling is lower than in the uniform waveguide. A third consideration is that n_{eff} varies with propagation distance. It is expected that with these additional considerations, the maximum theoretical coupling efficiency will be the same for either a tapered or conventional grating coupler.

Again referring to Figures 1-5, a weakness of ray tracing calculations is that the possibility of interference within the taper is ignored. Within the taper region the beam is not yet propagating at the mode propagation angle because it only reaches that angle as it exits the tapered portion of the waveguide. The result is that the roundtrip phase shift during propagation in this region is not equal to an integral number of wavelengths. This could allow for the possibility of interference in the tapered region. Interference does not occur because, in the propagating region, the wave vector direction is changed by 2α from each taper bounce. If the 2α change is large enough, interference does not occur.

The angular shift induced by the taper is not continuous, but rather a discrete function of the number of reflections within the taper. The effect of this on the Θ_p vs. Θ_i curve is that while the general shape remains the same as predicted by ray tracing, locally, the curve is discontinuous. Each continuous segment of the curve that intersects the intrinsic mode width contributes to the coupling efficiency as shown in Figure 11. The overall coupling is the sum of the contribution from each continuous section. To obtain a continuous distribution, it is necessary to convolve the efficiency curves being summed such that they become indistinguishable. This is achieved by minimizing the taper angle, α. Because the change in propagation angle is 2α for a single taper bounce, the magnitude should be restricted to much less than the intrinsic mode width, i.e., $2\alpha << 0.5°$ (see Figure 10).

If 2α is small, interference between different portions of a coupled beam that had a different number of reflections off the taper could occur. However, no evidence of this was seen in our experiments, down to a taper angle of 0.007°.

The gratings were fabricated on polished quartz substrates. The substrates were coated with photoresist, exposed with a spatially filtered HeCd (λ = 0.4416 μm) beam, and developed using an in-situ monitoring process. The resulting photoresist gratings were then reactive ion etched into the quartz to a depth of 120 nm. The photoresist was then removed and the substrate thoroughly cleaned.

The tapered films were fabricated by two different methods. The first method was electron beam vacuum deposition which was shadowed by a cleaved silicon wafer. The second method was variable speed dip coating of organic solutions of polycarbonate or titanium ethoxide.

The electron beam deposited films were made of zinc sulfide, ZnS. This film was chosen because of the high refractive index of 2.3, ease of evaporation, and low optical loss less than 4 dB/cm resulting from deposition at slow rates less than 1 nm/sec. The ZnS film thickness was 190 nm, slightly less than the TE_1 cutoff thickness for ZnS on quartz of 205 nm. A cleaved edge of a silicon wafer was placed between the substrate and the evaporation source. The distance between the substrate and the shadowing wafer was varied from 2 cm to 10 cm, depending on the taper length desired. The farther the shadowing wafer was from the substrate, the longer, and shallower, was the taper.

The first sample was shadowed from a distance of 10cm yielding a taper length of 1600 μm from full film thickness of 190 nm to zero thickness. For a linear taper those dimensions correspond to an α of 0.007°. However, a profilometer measurement of the taper reveals that the profile is more like a cosine curve (Figure 16). The sample was cleaved and a scanning electron microscope was used to view a cross section of the taper to determine how completely the film filled in the grating grooves. The first area observed was at the end of the taper where the film thickness was nearly zero. An area was viewed at the coupling edge of the grating to determine the roughness of the taper surface at the input coupling position. The grating grooves are more gradual on the taper at the input coupling position when compared to the initial grating profile.

The waveguide on the second ZnS sample was thicker than the first at 200 nm, and the wafer shadowing distance was reduced to 2 cm. The resulting taper distance was reduced to 100 μm, corresponding to a linear taper angle, $\alpha \cong 0.1°$.

The second method of variable speed dip coating of organic solutions was used on the third sample. The third sample was formed by dip coating a quartz substrate in polycarbonate. The substrate was dipped into a solution of polycarbonate dissolved in bromobenzene. The substrate was then slowly drawn at a constant velocity of approximately 100 μm/sec giving a thickness of 400 nm. At the appropriate position, the drawing speed was increased to 400 μm/sec. The faster drawing speed left a film thickness of about 210 nm, with the change

from 400 nm taking place over about 1000 μm corresponding to a linear taper angle α of 0.01°, but the profile was found to resemble exponential taper more than a linear taper.

Referring to Figures 17-21, the sample grating periods were all confirmed to be 0.36 μm by measurement of the first order Littrow angle. The samples were fabricated with two gratings so that each had a grating that was tapered and one untapered under the uniform waveguide region. The coupling efficiency at $\lambda = 0.6328$ μm for the untapered grating was measured as a function of the incidence angle, and the propagation angle of the mode within the waveguide was calculated. The tapers were fabricated so that the taper position relative to the edge of the coupler grating varied across the grating enabling measurement of coupling characteristics for a range of taper ratios on each grating.

The first sample, with the shallowest taper, supported coupling from the entire grating (e.g., the D_t/z_0 ratio did not exceed the maximum allowed for the mode). The acceptance range, η vs. Θ_i, was measured at four positions along the edge of the grating with the resulting efficiency curves shown in Figure 18. The second ZnS sample, with the steepest taper, supported coupling into the taper at only one edge (Figure 20). Because of the positioning of the taper, the polycarbonate sample couples into the taper at the position corresponding to the smallest taper ratio (Figure 21).

The efficiency curves of all samples were shifted to lower coupling angles relative to the untapered case as expected from the calculations. The acceptance-broadening by the samples was consistent with the dependence on taper angles predicted by the calculations. The first sample had an equivalent linear taper angle α of 0.007°. This meant that the angular shift induced by one reflection was 0.014°, which is much less that the FWHM of the intrinsic mode width of approximately 0.5° (Figure 10). For this reason, the convolution of many 0.5° wide efficiency curves centered 0.014° apart is essentially continuous. Therefore, the efficiency curves in Figure 18 are continuously broadened as expected from the ray tracing calculations.

Combining the measured coupling angle, tapered and untapered, with the model results as shown in Figure 11, allows calculation of the corresponding taper ratios. For the first sample, the four measured points were 13.2°, 11.6°, 8.2°, and 4.1°, and the untapered coupling angle was 19.5°. The corresponding taper ratios are calculated to be 0.320, 0.365, 0.415 and 0.456, respectively. Next, the corresponding Θ_p vs. Θ_i relationship is used to convert the untapered η vs. Θ_p acceptance curve (Figure 10) to a predicted acceptance curve for each measurement. These calculated curves are shown in Figure 18.

The second ZnS sample had an equivalent linear taper angle α of 0.1°. This results in a change in propagation angle within the waveguide of 0.2° for each bounce off the taper. This is equal to the FWHM of the η vs. Θ_p for propagation within the waveguide of approximately 0.2° (see Figure 19). The resulting efficiency curve is a convolution of 0.2° efficiency curves centered 0.2° apart, and therefore would be expected to oscillate with local maxima at distances 2α apart. The distances between local maxima were measured and averaged, with a resulting average value of 2α of 0.235°. This agrees with the value $\alpha \cong 0.1°$ measured by a profilometer.

The coupling angle shift exhibited in the second ZnS sample is near the onset of the substrate mode. The coupling efficiency appears to decrease fully before the onset of the substrate mode and therefore it is likely that the taper ratio is not so large that the substrate mode is interfering. This suggests that the taper ratio is slightly below 0.57.

The coupling shift exhibited by the third sample demonstrates that the effect of coupling with a taper ratio that is larger than the optimum is to couple into the substrate mode even though the propagation angle in the waveguide is far from cutoff. In this sample, the coupling angle is shifted a total of 4°, which is enough in this structure to shift the propagation angle so much that the substrate mode interferes. The efficiency curves of Figures 18-21 also indicate that the broadening trends found in other samples were also valid for lower refractive index films.

Wavelength acceptance-broadening is expected to correspond to the angular acceptance-broadening described above. The conversion from angular acceptance to wavelength acceptance is given by $\Delta\lambda = d \cos\Theta_i \Delta\Theta$, where ΔΘ is the coupling FWHM change in incidence angle and Δλ is the coupling FWHM change in wavelength. For the experimental case of Figure 18, where $D_t/z_0 = 0.456$, $d = 0.36$ μm, $\Theta_i = 4°$, and $\Delta\Theta = 2°$, the Δλ expected would be 12.5 nm. This is a high efficiency waveguide coupler suitable for diode lasers that have wavelength instabilities on the order of a few nm. The coupler is also readily fabricated in a single deposition process, and, unlike other grating coupler achromatization solutions, it has no additional components to align.

The ability to increase the angular acceptance of a grating coupler is very useful for many applications in integrated optics. For example, there is less alignment difficulty for grating couplers, and there is broader wavelength acceptance for laser diode applications. In addition, the grating/tapered film coupler has other less obvious possible uses, such as allowing the coupling angle for a given film to be shifted. For example, an optimized taper could have shifted the coupling angle of the first ZnS sample by more than 35°. Therefore, the coupling angle can be shifted without changing the period of the grating or the thickness of the film.

A shift in coupling angle could be useful in preventing interference of a substrate mode in the opposite di-

rection with that for the desired coupled mode. This problem arises in high index films where the coupling angle is so large in the positive direction that it passes the onset of the substrate mode in the opposite direction, thereby decreasing the coupling efficiency and possibly causing other detrimental effects. The problems are avoided by a taper shifting of the coupling angle below that of the reverse substrate mode.

The use of the grating/taper coupler combination in the same geometry as an output coupler results in the ability to spectrally disperse or converge the output beam depending on the taper orientation (similar to broadening or narrowing). The use of the taper to modify the coupler acceptance is not limited to grating couplers; the taper can be used to broaden or narrow the acceptance of a prism coupler in a similar manner.

It can now be appreciated that there has been presented a tapered structure that allows adjustment of the acceptance of a grating coupler over a wide range. The ratio of the transit distance in the taper to the projected taper length, D_t/z_0, has been shown to be the parameter for taper optimization. The qualitative taper profile must be taken into account when designing such a coupler, but any shape can be used if properly dimensioned. The taper distance, z_0, should be kept long (e.g., α should be kept small) to allow continuous, broadened efficiency curves.

The maximum acceptance-broadening (or narrowing) allowed occurs with higher index films and smaller period gratings. For the experimental sample of ZnS on quartz, the maximum relative broadening is 4.3 times that of an untapered grating structure. For one sample, a coupling FWHM of 2° was demonstrated. This agreed with the broadening predicted by ray tracing calculations. Conversely, the angular acceptance of a coupler can be narrowed by a corresponding amount (-4.3 in the above example). The experimental angular acceptance-broadening was equivalent to a wavelength broadening (FWHM) of 12.5 nm. This is a practical method for achromatizing a grating coupler, with minimal alignment or fabrication difficulties.

It can also be appreciated that there has been presented an optical diode laser structure wherein it is easy to use grating couplers, and wherein the difficulties with beam divergence and wavelength instability are eliminated. In the structure mode matching can be achieved and the outcoupled beam can be collimated or imaged clearly.

While the invention has been described with particular reference to a preferred embodiment, it will be understood by those skilled in the art that various changes may be made and equivalents may be substituted for elements of the preferred embodiment without departing from invention. For example, although the taper is thought of as a thickness change, it could also be a refractive index change. In addition, many modifications may be made to adapt a particular situation and material to a teaching of the invention without departing from the essential teachings of the present invention.

While the invention has been described with particular reference to a the combination of a tapered film and a grating coupler results in a hybrid coupler with an increased angular acceptance due to the taper, as well as the high efficiency and easier input beam positioning that are characteristic of the grating coupler. In addition, by positioning the taper differently, it can be used to decrease the acceptance of the coupler for applications where this is required.

As is evident from the foregoing description, certain aspects of the invention are not limited to the particular details of the examples illustrated, and it is therefore contemplated that other modifications and applications will occur to those skilled in the art. It is accordingly intended that the claims shall cover all such modifications and applications as do not depart from the true spirit and scope of the invention.

Claims

1. A hybrid optical waveguide structure, comprising:
   a substrate having a grating formed thereon; and
   a thin-film waveguide film being formed on said substrate and having a nonlinear portion overlaying said grating.

2. A hybrid optical waveguide structure, as set forth in Claim 1, wherein said nonlinear portion has a tapered profile.

3. A hybrid optical waveguide structure, as set forth in Claim 1, wherein said nonlinear portion has a cosine profile.

4. A hybrid optical waveguide structure, as set forth in Claim 1, wherein said nonlinear portion has an exponential profile.

5. A hybrid optical waveguide structure, as set forth in Claim 1, wherein said structure has a linear end portion and a nonlinear end portion with said grating disposed on said nonlinear end portion, and wherein said nonlinear portion of said waveguide film overlays said grating and decreases in profile near said nonlinear end portion of said structure.

6. A hybrid optical waveguide structure, as set forth in Claim 1, wherein said structure has a linear end portion and a nonlinear end portion with said grating disposed on said nonlinear end portion, and wherein said nonlinear portion of said waveguide film overlays said grating and increases in profile near said nonlinear end portion of said structure.

7. A hybrid optical waveguide structure, as set forth in Claim 1, wherein a nonlinear waveguide film portion angle, α, is the angle of incline or decline of the nonlinear portion of the waveguide film relative to the grating and substrate.

8. A hybrid optical waveguide structure, as set forth in Claim 7, wherein the angle α is positive when the film profile is decreasing in the grating area near the end of the nonlinear portion of the waveguide film.

9. A hybrid optical waveguide structure, as set forth in Claim 7, wherein the angle α is positive when the film profile is increasing in the grating area near the end of the nonlinear portion of the waveguide film.

10. A hybrid optical waveguide structure, as set forth in Claim 7, wherein the effect of angle α on a diffracted beam diffracted at an angle, Θ_d, relative to a substrate normal is that the diffracted beam is incident at a waveguide film surface at a propagation angle $\Theta_d+\alpha$ due to the nonlinear portion of the waveguide film.

11. A hybrid optical waveguide structure, as set forth in Claim 10, wherein the diffracted beam is reflected from the waveguide film surface and the reflected beam is incident at the substrate at a propagation angle of $\Theta_d+2\alpha$ relative to the substrate normal.

12. A hybrid optical waveguide structure, as set forth in Claim 11, wherein the 2α increase in propagation angle occurs for every reflection off the waveguide film surface.

13. A hybrid optical waveguide structure, as set forth in Claim 11, wherein the net result of the reflections is a shift in the propagation angle of $2\alpha n$, where n is the number of reflections off the film surface.

14. A hybrid optical waveguide structure, as set forth in Claim 7, wherein the length of the nonlinear portion of the waveguide film, z_0, is related to the α angle by

$$z_0 = \frac{t_f}{\tan(\alpha)}$$

where t_f is the waveguide film thickness.

15. A hybrid optical waveguide structure, as set forth in Claim 7, wherein an incident beam is diffracted off the grating at an interface of the waveguide film and substrate the diffracted beam undergoes total internal reflection off the nonlinear portion of the waveguide film, and wherein the nonlinear portion changes the propagation angle of the diffracted within the waveguide film such that upon leaving the nonlinear portion the diffracted beam is traveling at the correct propagation angle for the guided mode.

16. A hybrid optical waveguide structure, as set forth in Claim 15, wherein the nonlinear portion of the waveguide film changes the angular acceptance of the grating by diffracting the beam from the grating a number of bounces off the waveguide film, whereby each bounce changes the propagation angle in the waveguide film.

17. A hybrid optical waveguide structure, as set forth in Claim 16, wherein bouncing compensates for changes in propagation angle with incidence angle.

18. A hybrid optical waveguide structure, as set forth in Claim 16, wherein the nonlinear portion of the waveguide film changes the angular acceptance of the grating by shifting a grating angle of incidence induced by the bounces.

19. A hybrid optical waveguide structure, as set forth in Claim 18, wherein changing the angular acceptance of the grating by shifting the grating angle of incidence induced by bouncing lowers the value of angular

dispersion of the grating and reduces change in the diffraction angle due to change in the incidence angle.

20. A hybrid optical waveguide structure, as set forth in Claim 1, wherein said waveguide film is an inorganic material.

21. A hybrid optical waveguide structure, as set forth in Claim 1, wherein said waveguide film is zinc sulfide.

22. A hybrid optical waveguide structure, as set forth in Claim 1, wherein said waveguide film is an organic material.

23. A hybrid optical waveguide structure, as set forth in Claim 1, wherein said waveguide film is polycarbonate.

FIG.1

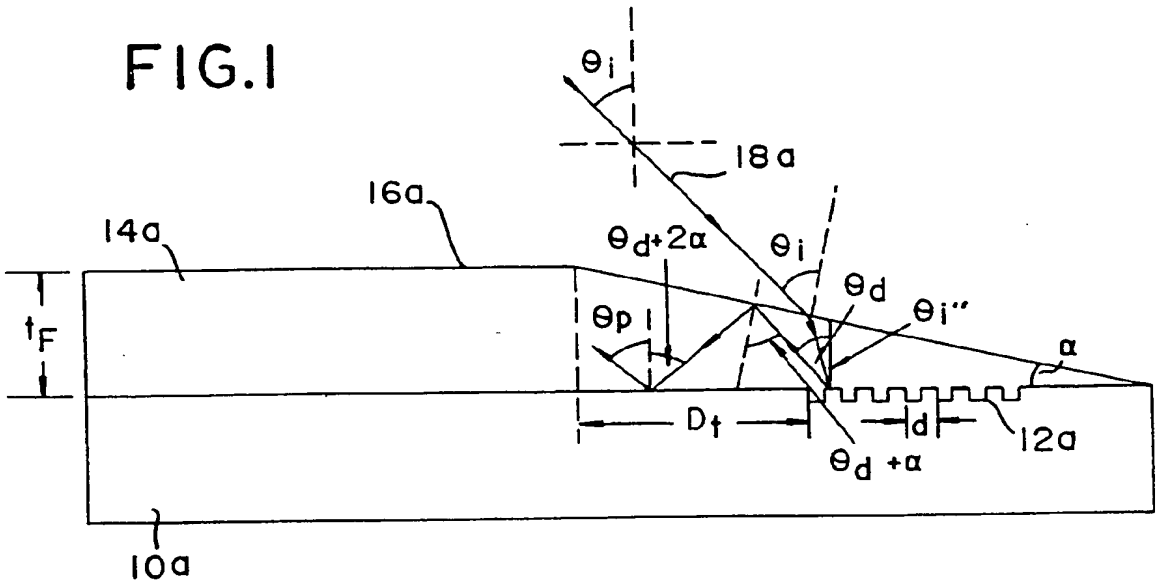
θi
18a
16a
14a
θd+2α
θi
θd
θi''
θp
α
tF
Dt
d
12a
θd +α
10a

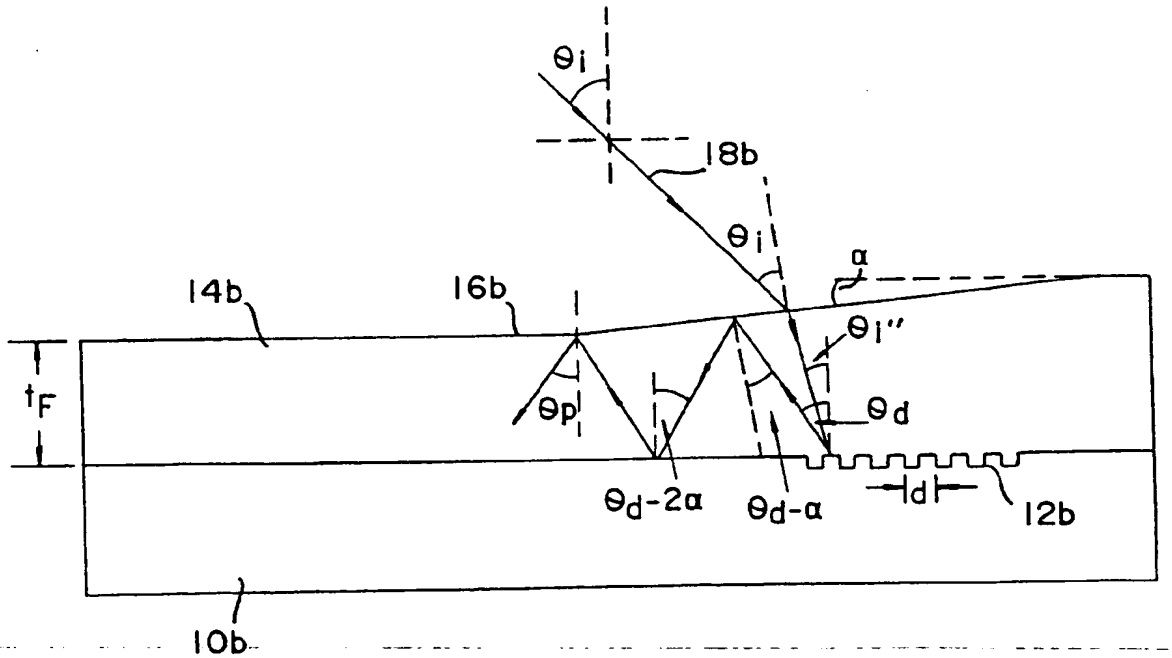
θi
18b
θi
α
14b
16b
θi''
tF
θp
θd
θd-2α
θd-α
d
12b
10b

FIG.2

FIG.3

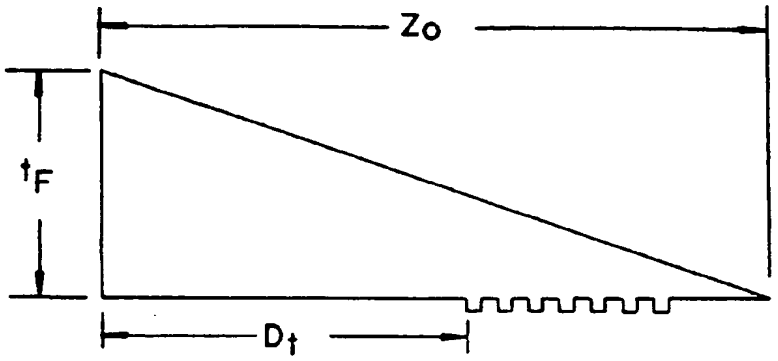

FIG.4

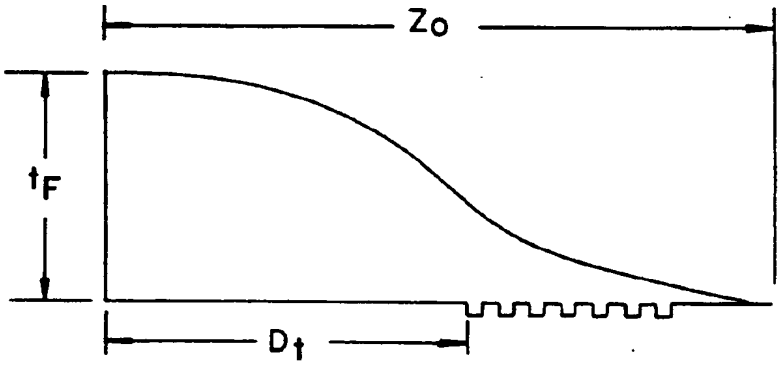

FIG.5

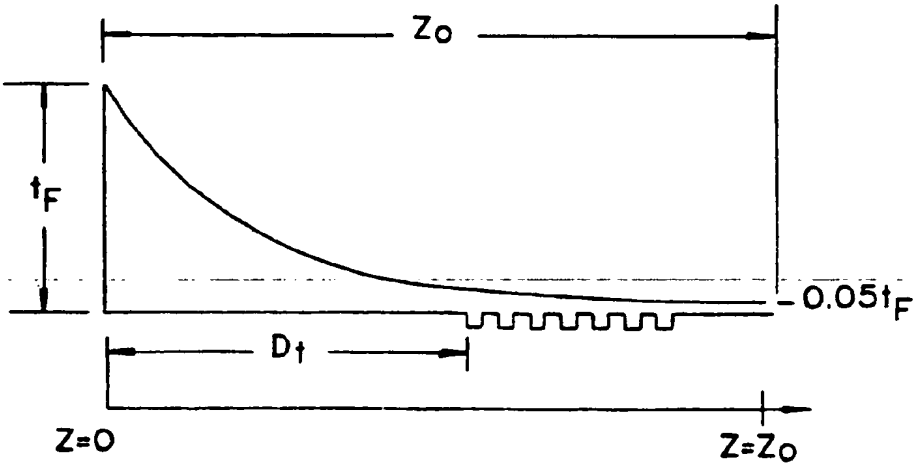

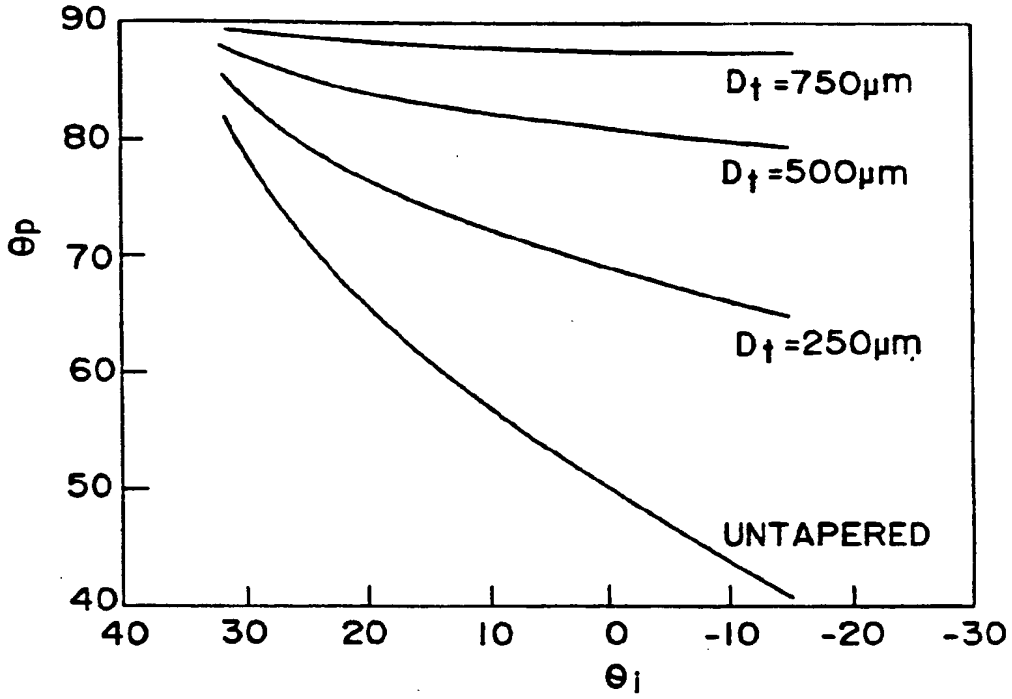
90
80
70
60
50
40
θp
Dt =750μm
Dt =500μm
Dt =250μm
UNTAPERED
40
30
20
10
0
-10
-20
-30
θi

FIG.6

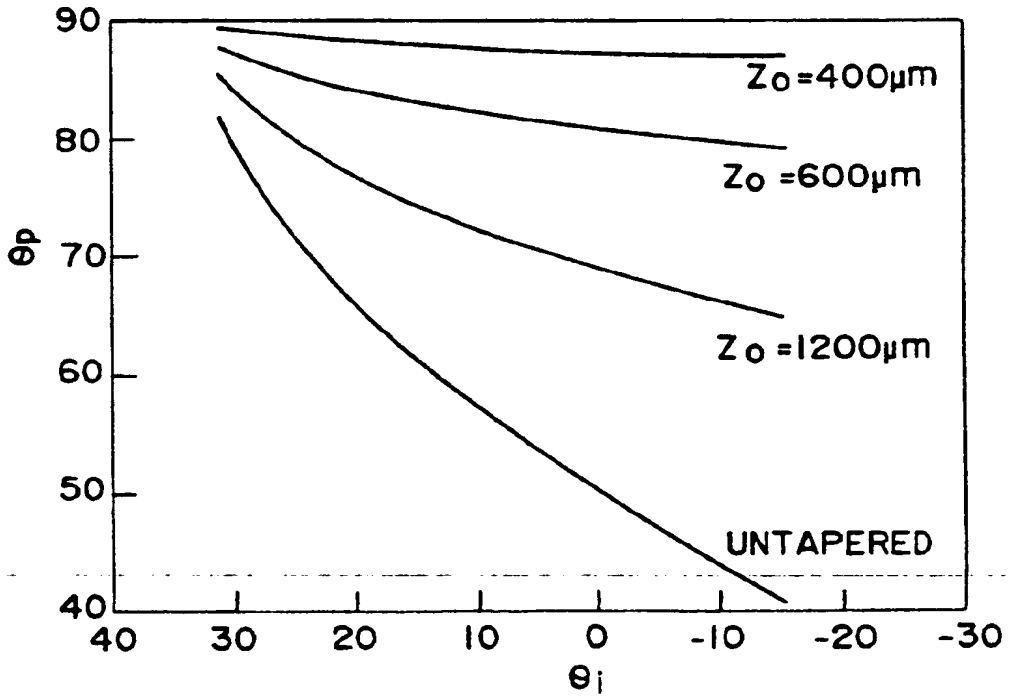
90
80
70
60
50
40
θp
Zo =400μm
Zo =600μm
Zo =1200μm
UNTAPERED
40
30
20
10
0
-10
-20
-30
θi

FIG.7

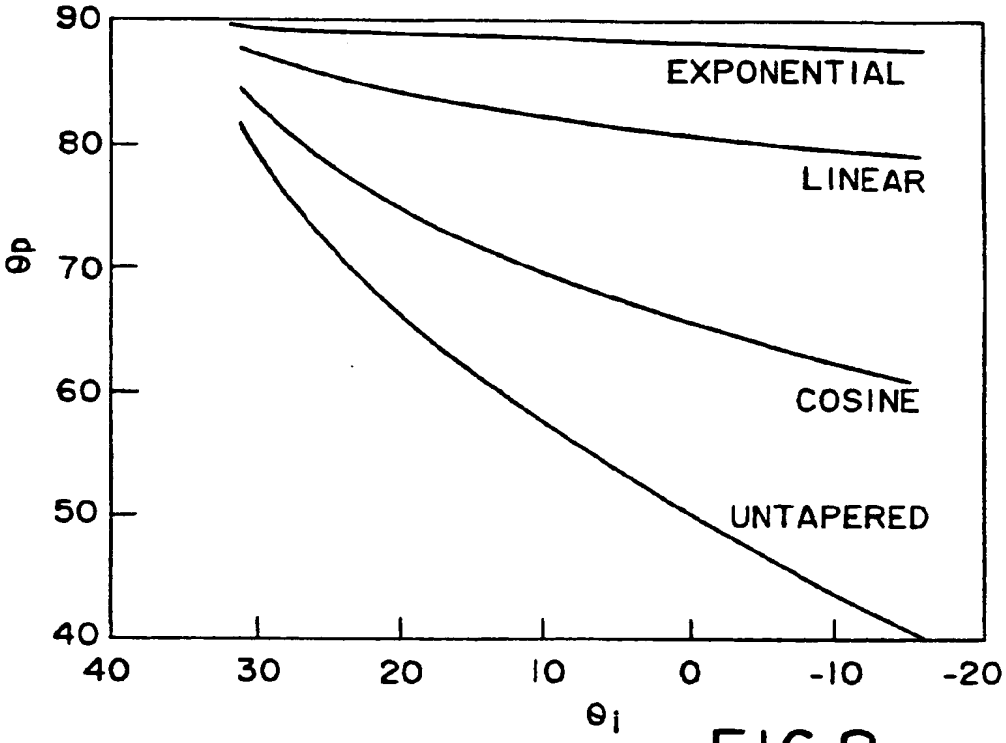
90
80
70
60
50
40
θp
EXPONENTIAL
LINEAR
COSINE
UNTAPERED
40
30
20
10
0
-10
-20
θi

FIG.8

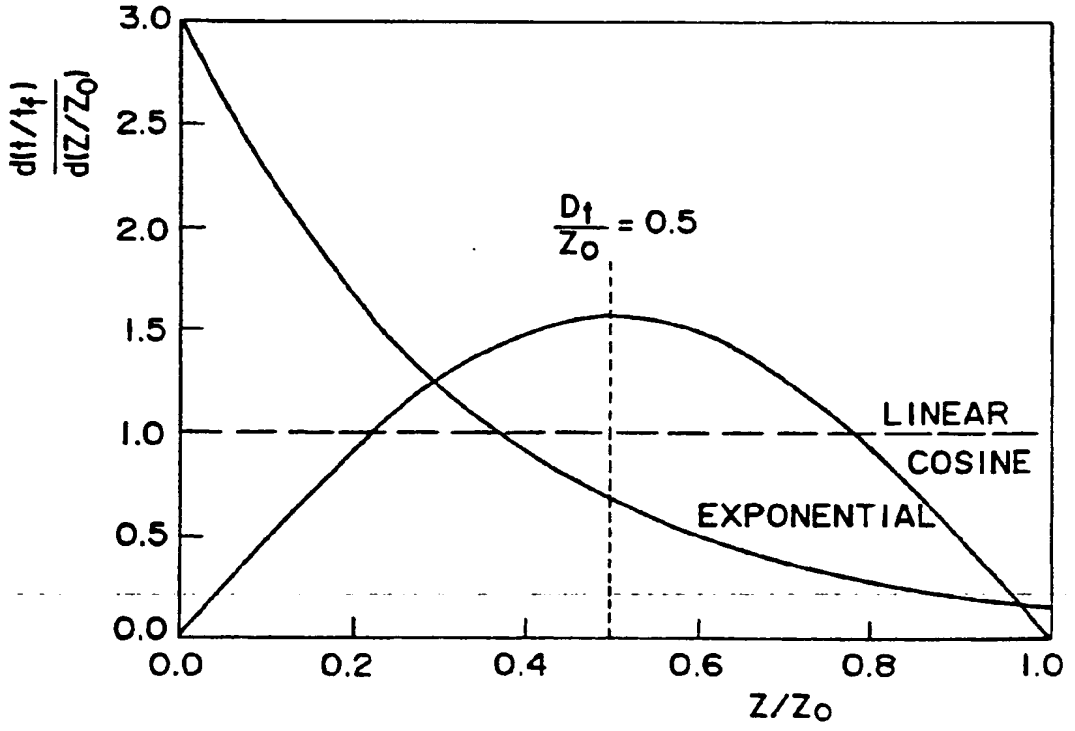
3.0
2.5
2.0
1.5
1.0
0.5
0.0
d(t/tf)
d(Z/Zo)
Dt/Zo = 0.5
LINEAR
COSINE
EXPONENTIAL
0.0
0.2
0.4
0.6
0.8
1.0
Z/Zo

FIG.9

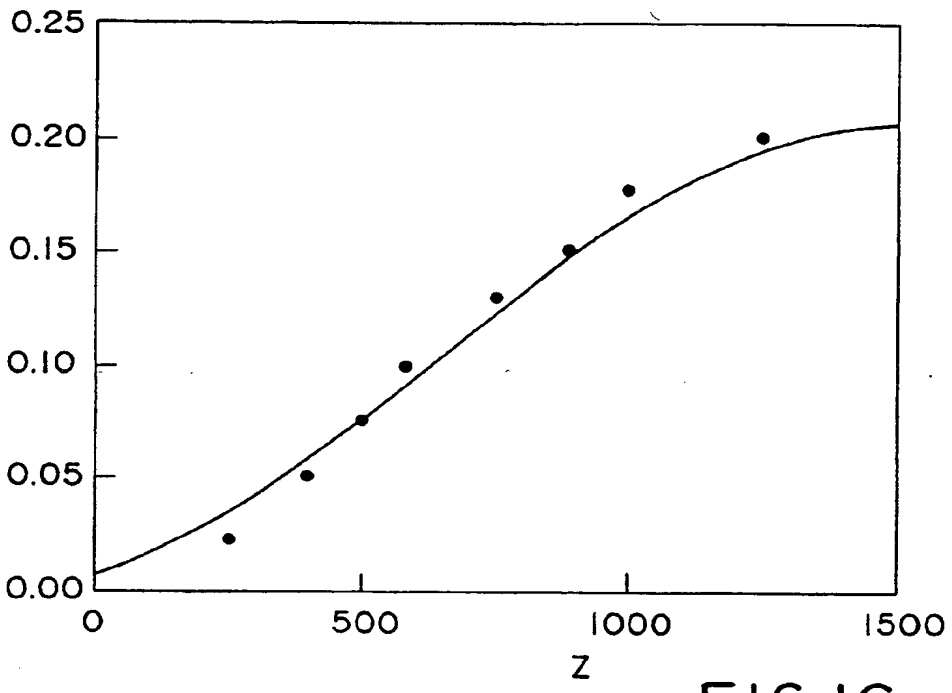

FIG.16

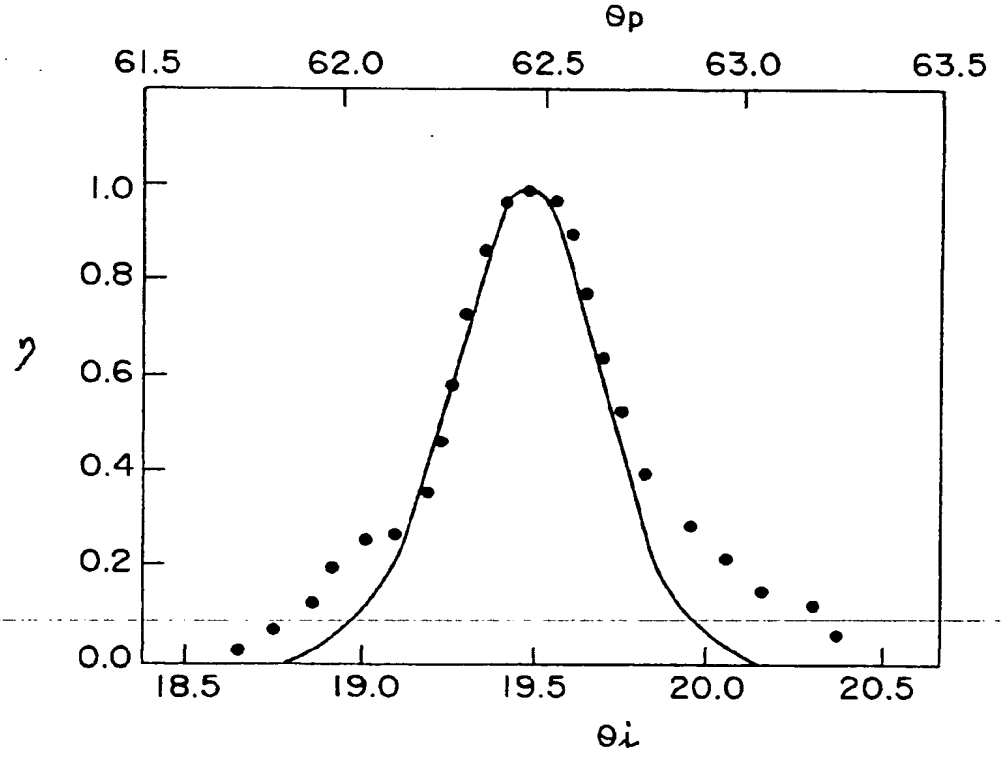

FIG.10

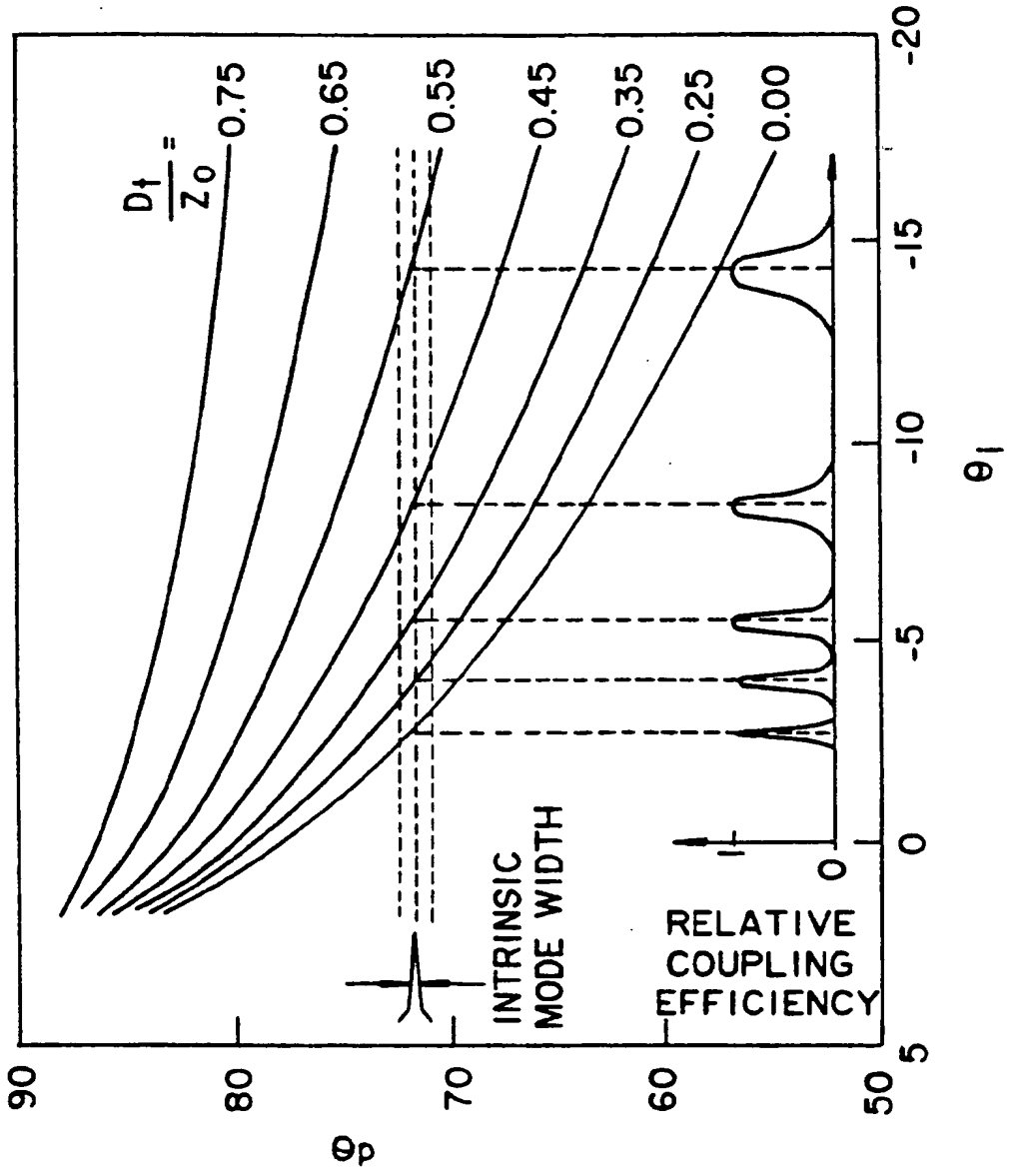

FIG.11

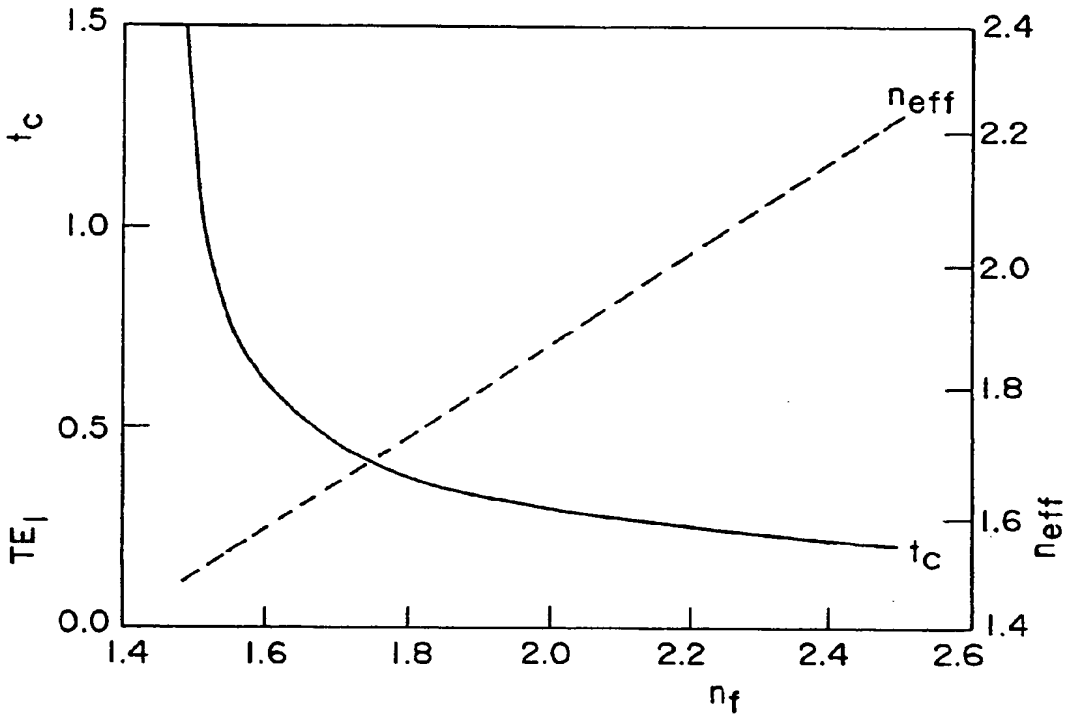

FIG.12

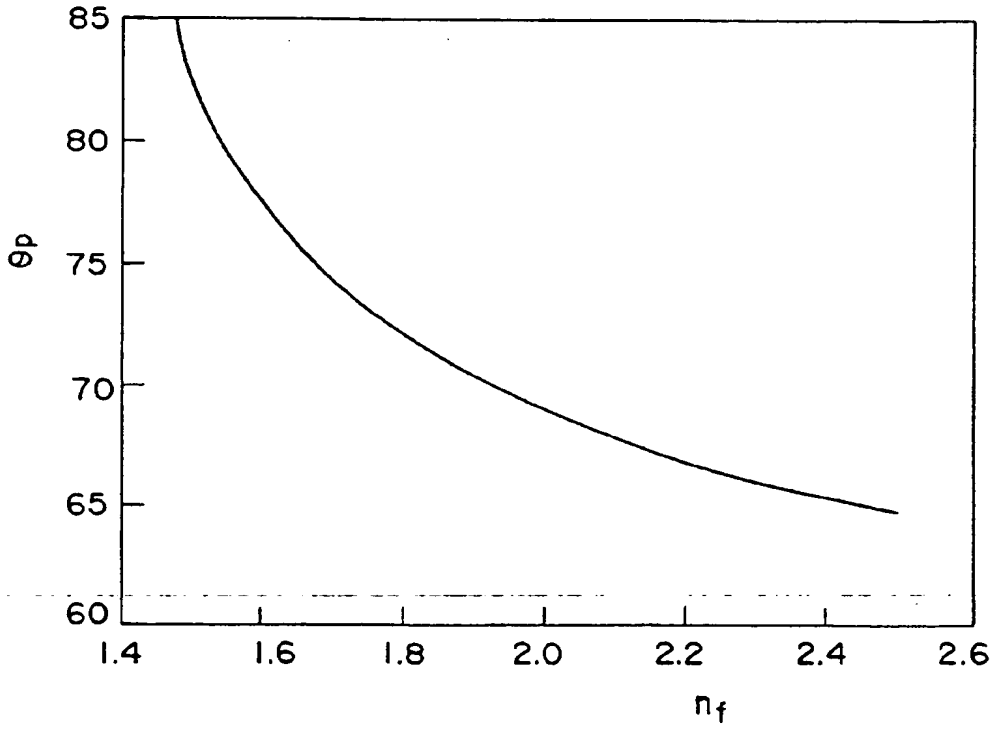

FIG.13

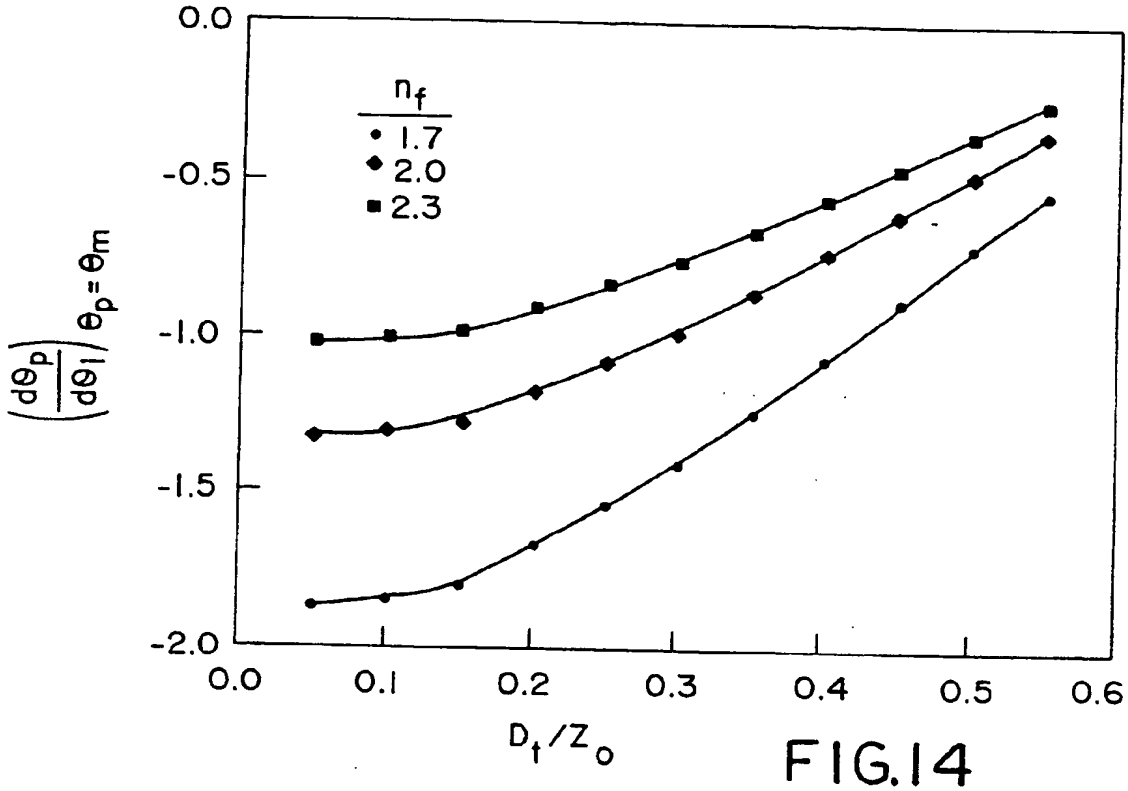
0.0
-0.5
-1.0
-1.5
-2.0
0.0
0.1
0.2
0.3
0.4
0.5
0.6
n_f
1.7
2.0
2.3
$\left(\frac{d\theta_p}{d\theta_I}\right)_{\theta_p=\theta_m}$
D_f/Z_o

FIG.14

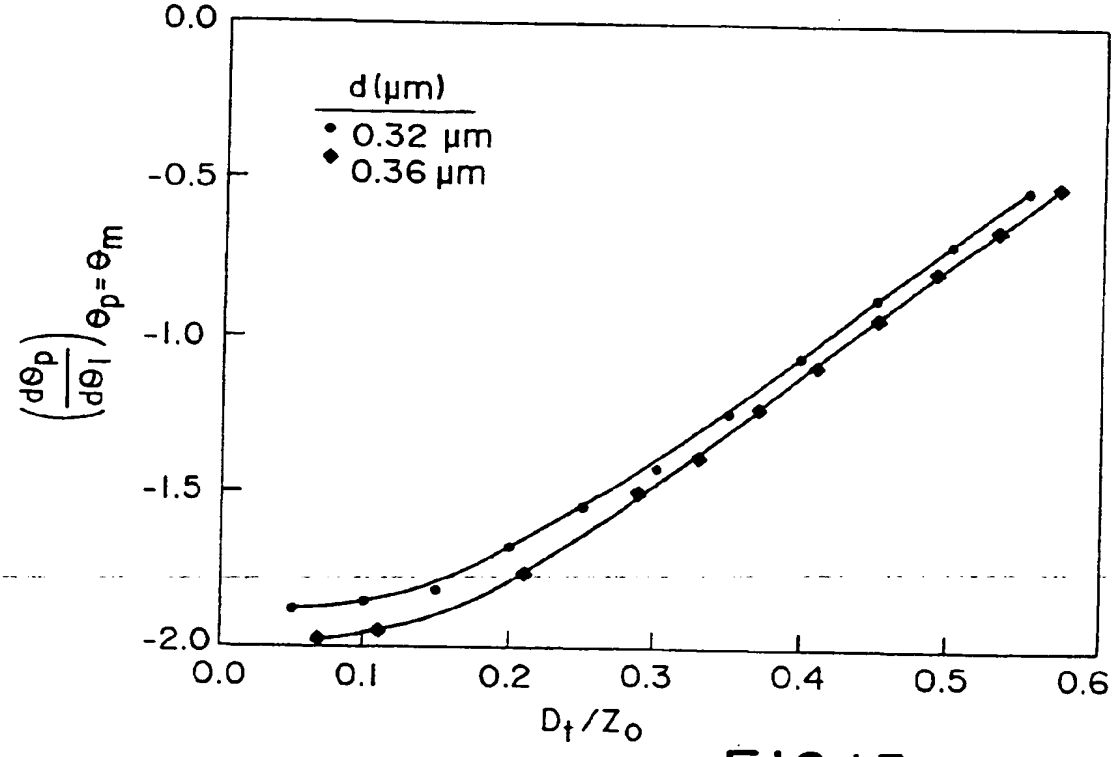
0.0
-0.5
-1.0
-1.5
-2.0
0.0
0.1
0.2
0.3
0.4
0.5
0.6
d(μm)
0.32 μm
0.36 μm
$\left(\frac{d\theta_p}{d\theta_I}\right)_{\theta_p=\theta_m}$
D_f/Z_o

FIG.15

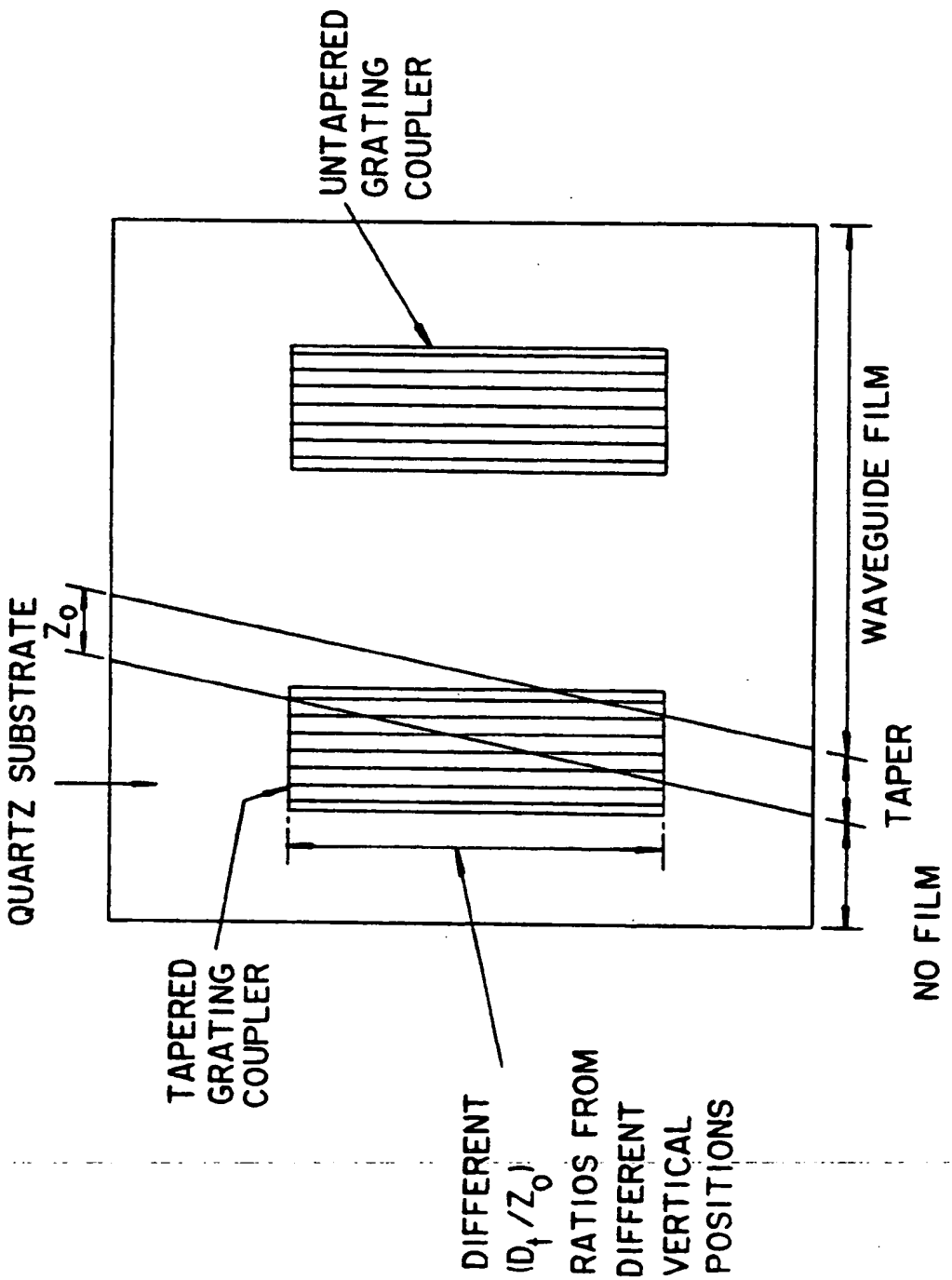

FIG.17

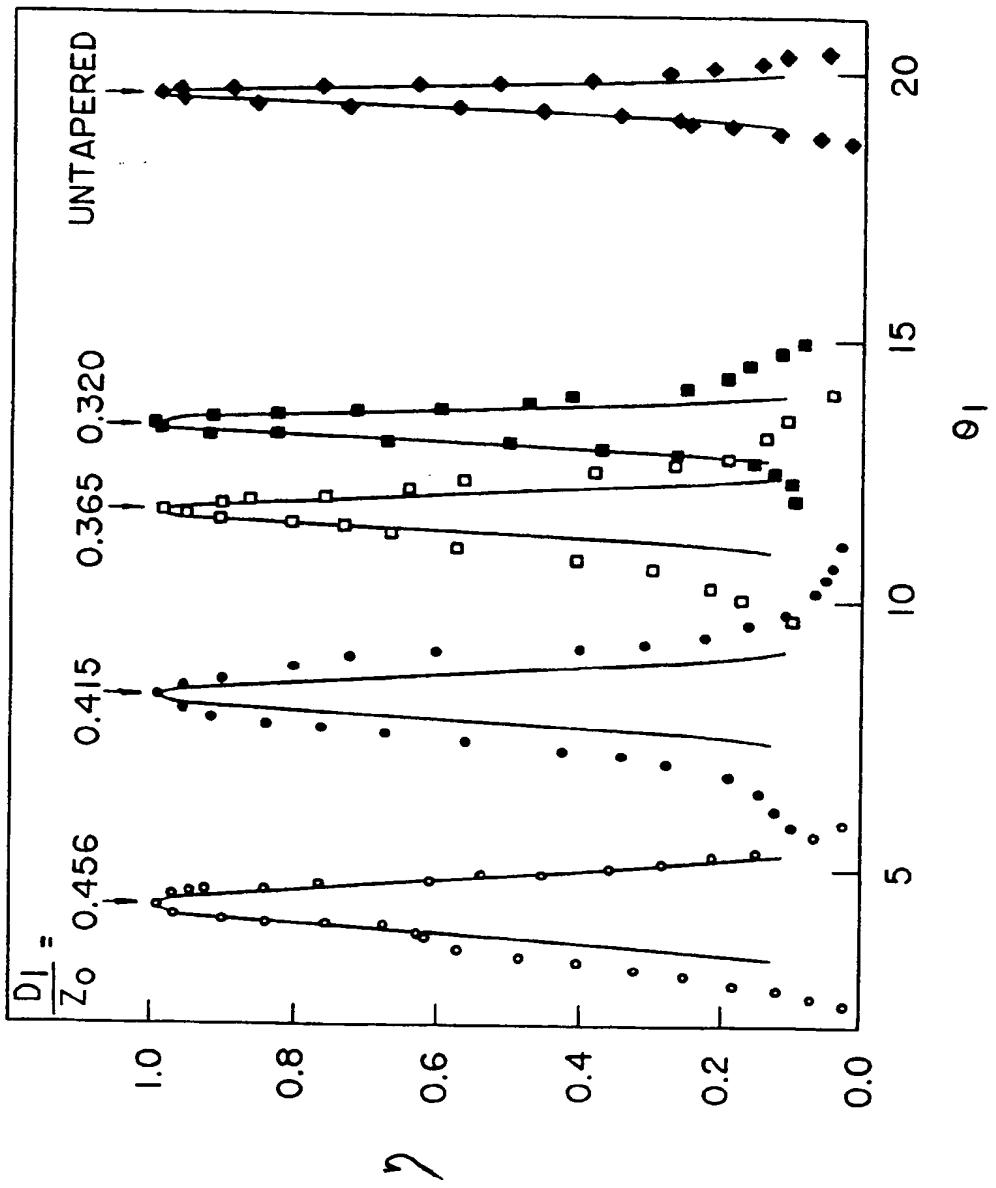
UNTAPERED
0.320
0.365
0.415
0.456
D1/Z0 =
1.0
0.8
0.6
0.4
0.2
0.0
η
5
10
15
20
θ1

FIG.18

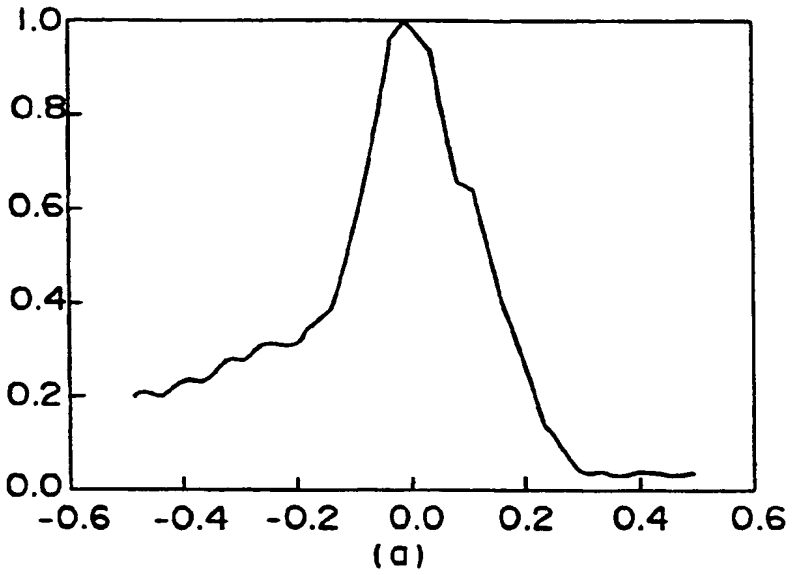
1.0
0.8
0.6
0.4
0.2
0.0
-0.6
-0.4
-0.2
0.0
0.2
0.4
0.6
(a)

FIG.19

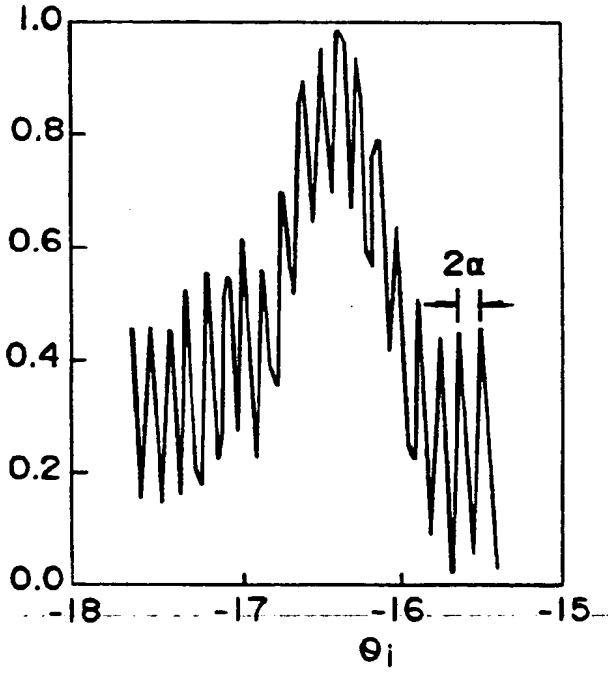
1.0
0.8
0.6
0.4
0.2
0.0
2α
-18
-17
-16
-15
θi
(b)

FIG.20

FIG.21

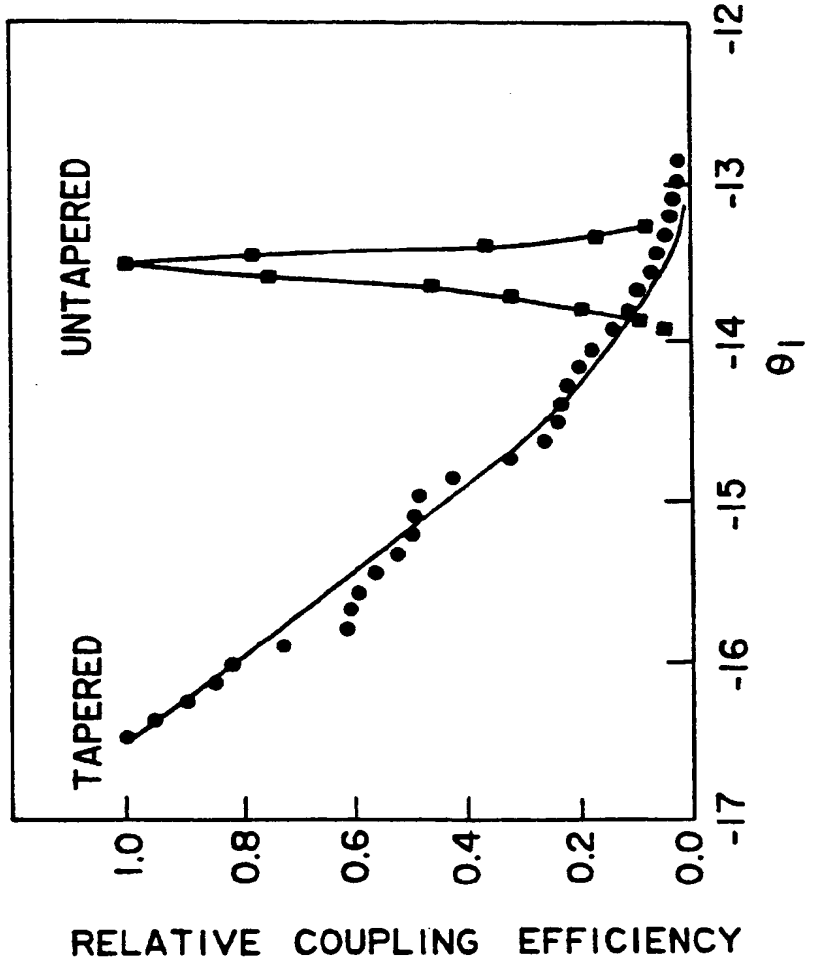
UNTAPERED
TAPERED
-12
-13
-14
-15
-16
-17
θ1
1.0
0.8
0.6
0.4
0.2
0.0
RELATIVE COUPLING EFFICIENCY

European Patent Office

EUROPEAN SEARCH REPORT

Application Number
EP 92 42 0412

DOCUMENTS CONSIDERED TO BE RELEVANT

Category	Citation of document with indication, where appropriate, of relevant passages	Relevant to claim	CLASSIFICATION OF THE APPLICATION (Int. Cl.5)
Y	EP-A-0 383 627 (SHARP K.K.) * column 2, line 49 - column 3, line 5 * * column 5, line 13 - line 34; figure 3B *	1,2,5	G02B6/12
A		7,8, 12-14,20	

Y	DE-A-3 536 497 (MITSUBISHI DENKI K.K.) * page 21, paragraph 1; figures 10B,11A *	1,2,5	

A	PATENT ABSTRACTS OF JAPAN vol. 12, no. 334 (P-756)8 September 1988 & JP-A-63 096 606 (MATSUSHITA ELECTRIC) 27 April 1988 * abstract *	1,2,5,7, 8,21,16, 20	

A	APPLIED OPTICS vol. 15, no. 7, July 1976, NEW YORK US pages 1681 - 1683 BOYD ET AL. 'Composite prism-grating coupler for coupling light into high refractive index thin-film waveguides' * page 1681 *	1,2,5,7, 8,10,11, 14-17	
			TECHNICAL FIELDS SEARCHED (Int. Cl.5)
	-----		G02B

The present search report has been drawn up for all claims

Place of search	Date of completion of the search	Examiner
BERLIN	19 FEBRUARY 1993	VON MOERS F.

CATEGORY OF CITED DOCUMENTS

X : particularly relevant if taken alone
Y : particularly relevant if combined with another document of the same category
A : technological background
O : non-written disclosure
P : intermediate document

T : theory or principle underlying the invention
E : earlier patent document, but published on, or after the filing date
D : document cited in the application
L : document cited for other reasons

& : member of the same patent family, corresponding document

EPO FORM 1503 03.82 (P0601)